Journal of Catalysis 283 (2011) 89–97

Contents lists available at SciVerse ScienceDirect

Journal of Catalysis

journal homepage: www.elsevier.com/locate/jcat

Catalytic hydrogenation of tertiary amides at low temperatures and pressures using bimetallic Pt/Re-based catalysts

R. Burch, C. Paun, X.-M. Cao, P. Crawford, P. Goodrich, C. Hardacre, P. Hu *, L. McLaughlin, J. Sá, J.M. Thompson *

School of Chemistry and Chemical Engineering, Queen's University, Stranmillis Road, Belfast, Northern Ireland BT9 5AG, UK

ARTICLE INFO

Article history:
Received 1 May 2011
Revised 19 July 2011
Accepted 20 July 2011
Available online 27 August 2011

Keywords:
Platinum
Rhenium
Bimetallic
Titania
Amide
DFT

ABSTRACT

Hydrogenation of tertiary amides, in particular, *N*-methylpyrrolidin-2-one, can be efficiently facilitated by a TiO_2-supported bimetallic Pt/Re catalyst at low temperatures and pressures. Characterisation of the catalysts and kinetic tests have shown that the close interaction between the Re and Pt is crucial to the high activity observed. DFT calculations were used to examine a range of metal combinations and show that the role of the uncoordinated Re is to activate the C=O and that of the Pt is as a hydrogenation catalyst, removing intermediates from the catalyst surface. The rate enhancement observed on the TiO_2 support is thought to be due to the presence of oxygen vacancies allowing adsorption and weakening of the C=O bond.

1. Introduction

Amines are an important class of organic compounds, with a wide range of applications including as dyes, solvents, additives, anti-foam agents, corrosion inhibitors, detergents and drugs. Tertiary amines have found applications as catalysts for use in the urethane industry, e.g. *N*,*N*-dimethylcyclohexylamine or alkyldimethylamine with typical applications as quaternary derivatives, amine oxides and betaines, which can be further used in the manufacture of disinfectants, wood treatment, personal care, oilfields and water treatment. As a result of the large number of applications, the development of new methods for the production of amines has been the focus of a large number of research studies.

A potentially simple method of forming amines is via the reduction of amides, which can be easily obtained from the reaction of carboxylic acids, acid anhydrides or acid chlorides with primary or secondary amines. However, amide functional groups are considered difficult to reduce [1] and, to date, catalytic reduction of amides has been problematic. Commonly, the reduction of amides is achieved using stoichiometric reducing agents such as lithium aluminium hydride, for primary and secondary amides [2], or borane [3–5], for secondary and tertiary amides, resulting in significant amounts of waste and issues with the workup. Reduction of amides using hydrogen gas in the presence of homogeneous or heterogeneous catalysts including copper chromite [6], rhenium metal [7] and group 8–10 transition metals [8,9] has been shown to be successful, but typically has required high temperatures of up to 260 °C and high pressures of 100–300 bar. In these cases, the rate and selectivity has been found to be strongly dependent on the structure of the amide, the metal catalyst and reduction conditions.

Dobson [10] reported the reduction of amides to form the corresponding amine with hydrogen at elevated temperature (175–225 °C) and moderate to high pressures (27.6–137.9 bar) using group 8/Re bimetallic catalysts on a range of carbon and silica supports. Although some good conversions were found, the selectivities were variable. Hirosawa et al. [11] also showed that the synergistic effects of rhenium, molybdenum or tungsten with rhodium or ruthenium facilitated amide reduction in both homogeneous and heterogeneous catalytic systems. In this case, reaction conditions of >150 °C and 100 bar hydrogen were employed with high selectivities obtained. Smith et al. [12] compared a range of bi- and trimetallic catalysts (consisting of combinations of A, B, C where A is chosen from Co, Fe, Ir, Pt, Rh or Ru; B from Cr, Mo, Re and V; and C from Cu, In and Zn) at temperatures below 200 °C and at pressures below 50 bar hydrogen (6–10 bar). Although some of the catalysts provided good selectivity, low conversions were found if the temperature was below 100 °C.

Other examples of amide hydrogenation include the use of copper chromite with a nucleophilic reagent [13] in the preparation of primary, secondary and tertiary amines from fatty amides. Using a

* Corresponding authors. Fax: +44 (0)28 9097 4687.
E-mail addresses: p.hu@qub.ac.uk (P. Hu), jillian.thompson@qub.ac.uk (J.M. Thompson).

0021-9517/$ - see front matter © 2011 Elsevier Inc. All rights reserved.
doi:10.1016/j.jcat.2011.07.007

2:1 ratio of $CuO:Cr_2O_3$ along with sodium methoxide, the authors obtained 91–99% yield and 91–98% selectivity at hydrogen pressures of 10–27 bar and 250 °C. Very mild reaction conditions can be employed for amide hydrogenation using PtO_2 in dilute HCl, with hydrogenation of *N*-methylpyrrolidin-2-one occurring at room temperature. However, a large amount of catalyst is needed, and the catalyst cannot be easily recycled due to the formation of Magnus' salt ($[Pt(NH_3)_4][PtCl_4]$) [9]. Recently, Beamson et al. [14] have reported the use of a range of heterogeneous Rh/Mo, Ru/Re and Rh/Re bimetallic catalysts, derived from zero-valent metal carbonyls for the selective hydrogenation of primary amides such as cyclohexane carboxamide. Therein, synergistic behaviour of the metals provided activity for the hydrogenation; however, pressures below 50 bar H_2 and temperatures $\leqslant$120 °C resulted in low conversions and selectivities. In addition, hydrogenation of amides to form alcohols and amines has recently been reported using homogeneous ruthenium complexes at 10 bar H_2 and 110 °C in THF [15].

Here, we report the use of bimetallic Pt–Re catalysts for the hydrogenation of the amide *N*-methylpyrrolidinone Scheme 1 under mild reaction conditions (120–160 °C and 5–30 bar hydrogen). The relationship between the structural characterisation of these catalysts and kinetic experimental results is presented along with DFT calculations providing a rationale for the high activity observed with this bimetallic catalyst.

2. Experimental

2.1. Catalysts and materials

All the chemicals, *N*-methylpyrrolidinone, hexane, tetrahydrofuran, diethylether, methanol, methyl *tert*-butyl ether, were purchased from Aldrich in $\geqslant$97% purity and were used without further purification. The gases, H_2, 5% H_2 in Ar and N_2, used in this work were purchased from BOC as >99% pure gases. Platinum nitrate (assay 15.14%) and perrhenic acid (assay 39.4%) solutions were supplied by Johnson Matthey. Alumina (γ type), ceria-zirconia (zirconium doped cubic ceria) and titania P90 were used as received from Ketjen Catalysts, Johnson Matthey and Nippon Aerosil, respectively.

The monometallic Pt and Re catalysts were prepared by incipient wetness impregnation. An appropriate mass of the required precursor, perrhenic acid solution or platinum nitrate solution, to give the desired wt% metal loading was diluted with sufficient doubly distilled deionised water (18 MΩ) to give a volume equal to the pore volume of the support used. The solution was added to the support in three portions of equal volume with stirring after each addition until thoroughly mixed. The product was then dried at 120 °C for 12 h followed by calcination at 500 °C for 4 h. The bimetallic catalysts were prepared by sequential incipient wetness impregnation (S.I.) or co-impregnation by incipient wetness (C.I.). In the case of sequential impregnation, following deposition of one metal, the catalyst was dried and calcined before the process was repeated for the second metal. After this deposition, the catalyst was again dried and calcined.

2.2. Characterisation

The surface area and pore volumes of the catalysts obtained by BET N_2 isotherm (Micromeritics ASAP 2010) are shown in Table 1. The metal loading of all the catalysts prepared (with the nominal wt% loadings given in the catalyst descriptor) was determined by ICP–OES (Perkin–Elmer Optima 4300), and the results are

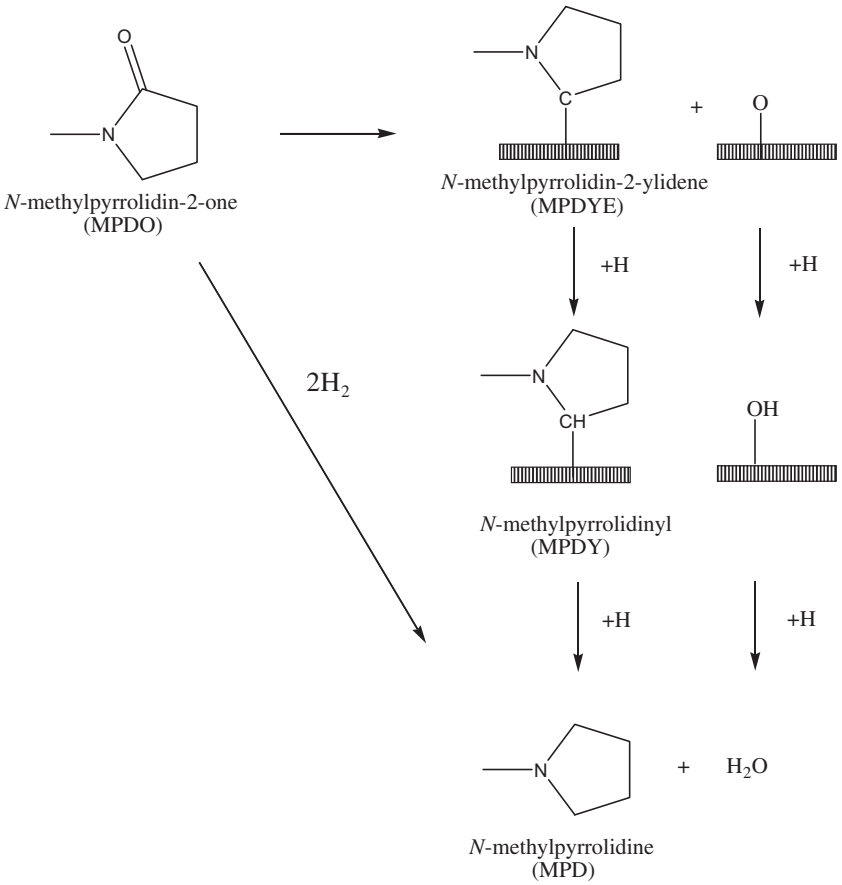

Scheme 1. Schematic reaction pathway for the catalytic hydrogenation of *N*-methylpyrrolidin-2-one (MPDO) to *N*-methylpyrrolidine (MPD) and water via an initial C=O cleavage followed by hydrogenation. (Possible intermediates: *N*-methylpyrrolidin-2-ylidene (MPDYE), *N*-methylpyrrolidinyl (MPDY).)

Table 1
Physical properties of the supports used and catalysts prepared.

Catalyst	Prep. method[a]	BET surface area ($m^2\ g^{-1}$)	Pore volume ($cm^3\ g^{-1}$)	Pt%[b]	Re%[b]
Al_2O_3	–	238	0.17	–	–
$CeZrO_4$	–	94	0.17	–	–
TiO_2	–	108	0.18	–	–
4 wt%Pt–4 wt%Re/Al_2O_3	S.I.	226	0.17	3.8	4.3
	C.I.	236	0.17	3.7	3.9
4 wt%Pt–4 wt%Re/$CeZrO_4$	S.I.	70	0.17	3.8	3.9
	C.I.	65	0.17	3.2	4.1
4 wt%Pt–4 wt%Re/TiO_2	S.I.	53	0.16	4.3	3.5
	C.I.	60	0.15	4.3	4
4 wt%Re–4 wt%Pt/TiO_2	S.I.	55	0.17	4.3	3.7
4 wt%Pt–1 wt%Re/TiO_2	S.I.	38	0.14	4.6	1.8
4 wt%Pt–0.25 wt%Re/TiO_2	S.I.	65	0.22	5.4	0.5
4 wt%Pt/TiO_2	–	83	0.20	4	–
4 wt%Re/TiO_2	–	63	0.22	–	3.8

[a] S.I. = sequential impregnation. C.I. = co-impregnation.
[b] Weight% loading as determined by ICP–OES.

presented in Table 1. As expected, the results show a decrease in the surface area of the catalyst after metal deposition.

The temperature-programmed reduction (TPR) (Micromeritics Autochem 2910) was measured by placing approximately 0.1 g of catalyst in a U-shaped tube, which was cooled to −50 °C in argon. The catalyst was reduced using 5% H_2 in Ar with the temperature being ramped from −50 to 800 °C at a rate of 5 °C min^{-1} and the hydrogen uptake monitored by a thermal conductivity detector (TCD). Powder XRD measurements were obtained using Cu Kα radiation (PANalytical X'PERT PRO MPD X-ray diffractometer).

2.3. Typical reaction procedure

The hydrogenation reactions were performed in an Autoclave Engineers 200 cm^3 stainless-steel stirred-tank reactor. The reactor was charged with catalyst (typically 0.2 g – sieved before reaction to between 50 and 250 μm) and solvent (15 cm^3), and the vessel purged three times with nitrogen before the reaction mixture was heated to the reduction temperature, 120 °C, with stirring (1500 rpm). The autoclave was charged with 20 bar hydrogen pressure, and the reaction mixture was left to stir for 1 h to pre-reduce the catalyst. Thereafter, the reactor was cooled to room temperature, depressurised and charged with amide (0.0052 mol), decane as an internal standard (0.001 mol) together with an additional 15 cm^3 of solvent. The reactor was heated under a nitrogen atmosphere to the desired reaction temperature (typically 120 °C) and pressurised to reaction pressure (typically 20 bar) at which point the reaction was started by starting the stirrer (typically 1500 rpm) and taking a sample of the liquid phase corresponding to $t = 0$. Hydrogen was supplied to the reactor by means of a delivery system connected to the reactor, thus guaranteeing a constant pressure of gas in the autoclave throughout the course of the reaction. Samples were taken at regular intervals, and analysed by an Agilent GC-FID using a DB-1 capillary column and GC–MS (Agilent) using a RTX-5 capillary column. Unless otherwise stated, the catalysts used/characterised were those prepared by sequential impregnation using platinum deposited on a rhenium-based catalyst with the nominal metal loading of each metal being 4 wt%.

2.4. Density Functional Theory (DFT) calculations

All periodic DFT calculations with Perdew–Burke–Ernzerhof (PBE) generalised gradient approximation (GGA) functional [16] were performed using Vienna *ab initio* simulation program (VASP) [17,18]. The projector-augmented-wave (PAW) pseudopotentials [19] were utilised to describe the core electron interactions with a 400 eV cut-off energy of plane-wave basis set.

All the models were simulated as a periodic 4-layer slab with a ~12 Å vacuum separating neighbouring slabs in the Z direction, in which adsorbates and top two layers were relaxed and the others were fixed. The energies of all the intermediates involving two species were calculated in two separate unit cells. Forces on relaxed atoms were less than 0.05 eV $Å^{-1}$, after the geometry optimisation. The Re flat surface was modelled by a close-packed (0001) facet. A $p(3 \times 3)$ supercell was used with corresponding $3 \times 3 \times 1$ Monkhorst–Pack k-point mesh for Brillouin zone sampling. The stepped surfaces of Pt and Rh were modelled by a (211) facet. A $p(1 \times 3)$ unit cell was used with a $4 \times 3 \times 1$ Monkhorst–Pack k-point mesh. The stepped surfaces of Re and Ru were modelled by removing two neighbouring rows of atoms on the top layer of (0001) facets. A $p(5 \times 3)$ unit cell was used with $2 \times 3 \times 1$ Monkhorst–Pack k-point mesh. The two-phase Re/X (X: Pt, Pd, Rh or Ru) was modelled with a $p(3 \times 3)$ Re monolayer terrace on a $p(5 \times 3)$ 3-layer X-metal flat surface substrate. The Re terrace was covered with 1 monolayer (ML) oxygen excluding the step edge sites in the Re/X interface. The Brillouin zone was sampled with $2 \times 3 \times 1$ Monkhorst–Pack k-point mesh. The five lowest energy structures from the results of Nose thermostat molecular dynamics simulation ($T = 120$ °C, 2 fs per step, 1000 steps) were selected to be further optimised by conjugate gradient methods for Re/X systems. The lowest energy structure was then utilised for all subsequent studies. Transition states (TSs) of reactions were located using the constrained minimisation method [20–22].

The reaction free energy was calculated as follows:

$$\Delta G = \Delta E - T\Delta S$$

where ΔE denotes the reaction energy from DFT, and ΔS is the entropy change from the gas or liquid phase to the adsorption on the surface. For a gas-phase molecule, its entropy is directly calculated in terms of the statistical thermodynamics formulae of a classical ideal gas [23], and for a liquid molecule, its entropy S_l is calculated by correcting its gaseous entropy S_g in the standard pressure P^o with the gas vapour P^* in the ideal solution via:

$$S_l = S_g + RT\ln(P^*/P^o)$$

3. Results

3.1. Catalyst testing

A range of bimetallic Pt/Re catalysts supported on $CeZrO_4$, TiO_2 and Al_2O_3 were prepared and tested for the selective hydrogenation of *N*-methylpyrrolidin-2-one to *N*-methylpyrrolidine. Fig. 1 shows the conversion with respect to time at 120 °C and 20 bar

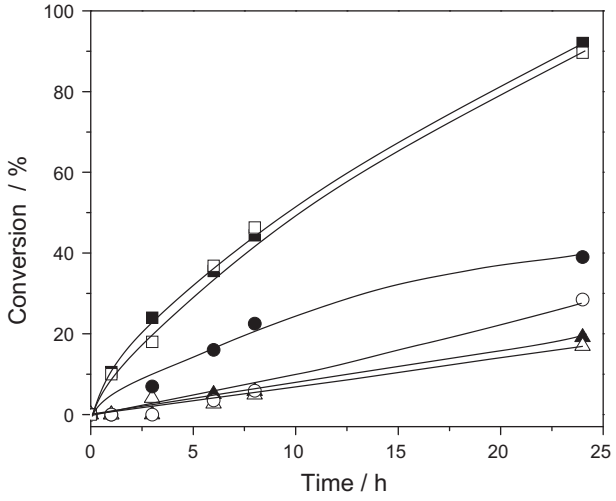

Fig. 1. Variation of amide conversion as a function of time for the hydrogenation of *N*-methylpyrrolidin-2-one at 120 °C, 20 bar H_2, stirred at 1500 rpm in hexane using (□) 4 wt%Pt–4 wt%Re/TiO_2 C.I., (■) 4 wt%Pt–4 wt%Re/TiO_2 S.I., (○) 4 wt%Pt–4 wt%Re/Al_2O_3 C.I., (●) 4 wt%Pt–4 wt%Re/Al_2O_3 S.I., (Δ) 4 wt%Pt–4 wt%Re/$CeZrO_4$ C.I. and (▲) 4 wt%Pt–4 wt%Re/$CeZrO_4$ S.I.

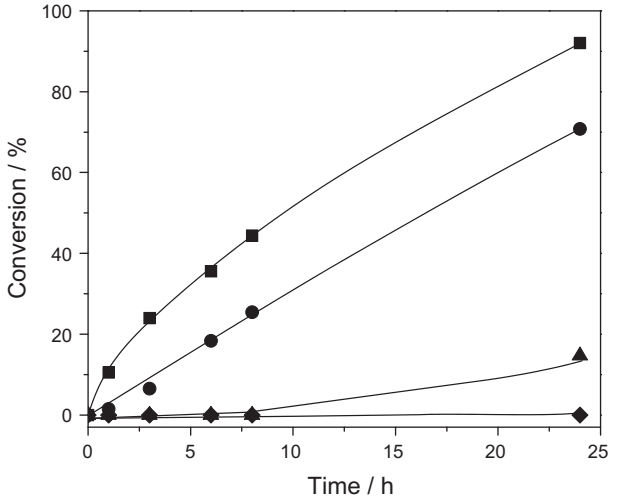

Fig. 2. Variation of amide conversion as a function of time for the hydrogenation of *N*-methylpyrrolidin-2-one at 120 °C, 20 bar H_2, stirred at 1500 rpm in hexane using (■) 4 wt%Pt–4 wt%Re/TiO_2 S.I., (●) 4 wt%Re–4 wt%Pt/TiO_2 S.I., (▲) 4 wt%Pt/TiO_2 and (♦) 4 wt%Re/TiO_2.

H_2 pressure using hexane as the solvent. For the supported 4 wt% Pt–4 wt% Re catalysts some activity was observed in all cases, but the TiO_2-supported catalyst showed almost complete conversion after 24 h. Significantly lower activity was observed for both $CeZrO_4$ and Al_2O_3 supports. Neither the surface areas or pore volumes of the catalysts examined (Table 1) can be correlated with their activity showing that these are not fundamental factors in achieving high conversions and selectivities. A 100% selectivity to *N*-methylpyrrolidine was found for all platinum–rhenium supported catalysts. Little activity for the bare supports was observed with the exception of the $CeZrO_4$ support, where 10% conversion was found after 20 h and, in this case, 49% selectivity to the amine was observed with the balance found to be 1-butanol. Some variation was found with the method of preparation between co-impregnation and sequential impregnation, with the latter showing higher activity, in general; however, this variation is minor compared with the effect of the support. In contrast to the bimetallic catalysts, the monometallic TiO_2-supported catalysts showed low activity, Fig. 2. Both 4 wt%Pt/TiO_2 and 4 wt%Re/TiO_2 catalysts showed little conversion after 7 h. In the case of the platinum-based catalyst, after 24 h, ~15% conversion was achieved, again with 100% selectivity to the amine.

The effect of the impregnation sequence of Pt and Re on the conversion and selectivity was also studied. Fig. 2 shows the kinetic profiles obtained when using catalysts, where Re was sequentially impregnated onto a Pt/TiO_2 catalyst (denoted Re–Pt/TiO_2) and where Pt was sequentially impregnated onto a Re/TiO_2 catalyst (denoted Pt–Re/TiO_2); for each metal, the loading used was 4 wt%. Both preparation sequences produced highly active catalysts. Although platinum deposition on a rhenium-based catalyst resulted in a higher final conversion compared with the reverse sequence of impregnation, the difference is due to the increased activity in the first 3 h of reaction, with both catalysts showing similar activity after this stage. In each case, >80% conversion was found after 24 h, and no change in the selectivity was observed.

Clearly, the presence of Re and Pt together is critical in providing an active catalyst. Fig. 3 shows the effect of varying the Re loading, whilst maintaining the loading of Pt at 4 wt%. A significant increase in the activity of the catalyst was observed with Re loading from a nominal 0.25 wt% (ICP 0.55 wt%) to 1 wt% (ICP 1.8 wt%),

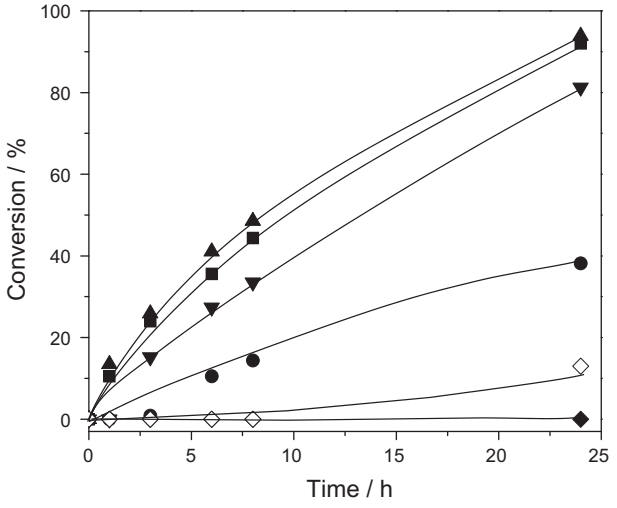

Fig. 3. Variation of amide conversion as a function of time for the hydrogenation of *N*-methylpyrrolidin-2-one at 120 °C, 20 bar H_2, stirred at 1500 rpm in hexane using (■) 4 wt%Pt–4 wt%Re/TiO_2, (▲) 4 wt%Pt–1 wt%Re/TiO_2, (▼) 4 wt%Pt–0.5 wt%Re/TiO_2, (●) 4 wt%Pt–0.25 wt%Re/TiO_2, (♦) 1 wt%Pt–0.25 wt%Re/TiO_2 and (◇) 4 × 1 wt%Pt–0.25 wt%Re/TiO_2.

with the initial rates increasing from 0.096 mmol h^{-1} g_{cat}^{-1} to 3.2 mmol h^{-1} g_{cat}^{-1}; however, no further rate enhancement was found on increasing the Re loading to 4 wt% (ICP 3.5wt%), where the initial rate was 3.1 mmol h^{-1} g_{cat}^{-1}. To determine the effect of dispersion, a catalyst was prepared with lower metal loadings, but maintaining the ratio Pt:Re at 4:1. 1 wt%Pt–0.25 wt%Re/TiO_2 was not found to be very active even on increasing the overall catalyst mass used from 0.2 g to 0.8 g to ensure the same amount of metal present in the reaction mixture compared with the reaction catalysed by 4 wt%Pt–1 wt%Re/TiO_2, Fig. 3. This implies that the lower activity of the low-loading catalyst may be due to insufficient contact between the Re and Pt due to the higher dispersion compared with the higher loaded catalysts.

The catalytic testing has shown that although the critical interaction required for the amide hydrogenation is between the platinum and the rhenium, the presence of titania can promote the activity of the catalyst. Catalysts based on metals supported on

reducible oxides, particularly TiO_2, have been studied extensively due to the ability of the metal to induce facile reduction of the oxide support and form oxygen vacancies. For example, in the catalysts studied herein, the Ti^{4+} is reduced to Ti^{3+} under hydrogen even at low temperature. This activates the support and allows both the metallic and oxidic phases to participate in C=O bond hydrogenation reactions, whereby the C=O bonds are thought to interact with the exposed Ti^{3+} sites on the support or oxygen vacancies [24–26]. A similar mechanism is thought to be in operation for the amide hydrogenation.

3.2. Reaction kinetics

To ensure that the kinetics obtained were in the intrinsic kinetic regime, a study into mass transfer limitations using the 4 wt%Pt–4 wt%Re/TiO_2 catalyst prepared by sequential impregnation was carried out in hexane for the hydrogenation of *N*-methylpyrrolidin-2-one. The speed of agitation was varied between 800 and 2000 rpm with no change in the reaction rate observed above 1500 rpm, Fig. S1, indicating the absence of gas to liquid mass transfer at the rotation speed of 1500 rpm used in these studies. The kinetics showed a linear dependence of the initial rate of reaction with the catalyst mass, Fig. S2, indicating that liquid to solid mass transfer limitations are negligible at the catalyst mass of 0.2 g typically used. Fig. S3 shows the Arrhenius plot between 120 °C and 160 °C, below which the amide solubility was limited in the hexane solvent, and an apparent activation energy of 56 kJ mol^{-1} was determined indicating that the rates obtained are predominantly kinetically controlled. It should be noted that no change in the selectivity was observed over these experimental conditions, with the only product observed being *N*-methylpyrrolidine. At the amide concentrations studied herein (0.017–0.183 M), the reaction was found to be zero order in amide, Fig. S4, and first order in hydrogen, Fig. S5. Above 0.183 M, the rate of reaction dropped dramatically due to the maximum solubility of the amide in hexane being exceeded. Under these experimental conditions, the catalyst aggregates in the polar amide phase and was no longer found to be evenly distributed throughout the liquid phase even on strong mixing.

3.3. Catalyst characterisation

Fig. 4 shows the TPR characterisation of the 4 wt%Pt–4 wt%Re catalysts supported on titania, alumina and ceria-zirconia and, for comparison, the TPR of 4 wt%Pt/TiO_2 and 4 wt%Re/TiO_2. The TPR analysis of the 4 wt%Pt–4 wt%Re/TiO_2 catalyst shows three peaks at 3 °C, 40 °C, and 400–600 °C. The first two features are attributed to reduction of Pt only, in agreement with the TPR of the 4 wt%Pt/TiO_2 catalyst, and oxygen at the interface between Pt and Re, which would indicate a significant interaction between the Pt and Re. Similar high temperature features, albeit showing a maximum reduction at a lower temperature of 315 °C and a second peak at 380 °C, is found with 4 wt%Re/TiO_2. These high temperature peaks could be due to the reduction of ReO_x [27] and/or reduction of the bulk titania support. The ceria-zirconia-supported bimetallic catalyst shows one peak at ~65 °C, which could be attributed to reduction of Pt only [28] or, as found for the TiO_2-based catalyst, the interfacial oxygen between Pt and Re. A similar assignment of the low-temperature peaks between 50 and 125 °C for the alumina supported catalyst is likely [29]. The TPR is in good agreement with recently reported EXAFS results on these systems [30], which shows that under both gas phase and liquid phase reduction of the catalysts, the predominant state of the both Pt and Re are zero valent, irrespective of the support used. There is little evidence of Re or Pt in the XRD patterns of any of the catalysts shown in Fig. S6, which is likely due to the metal particle size being extremely small.

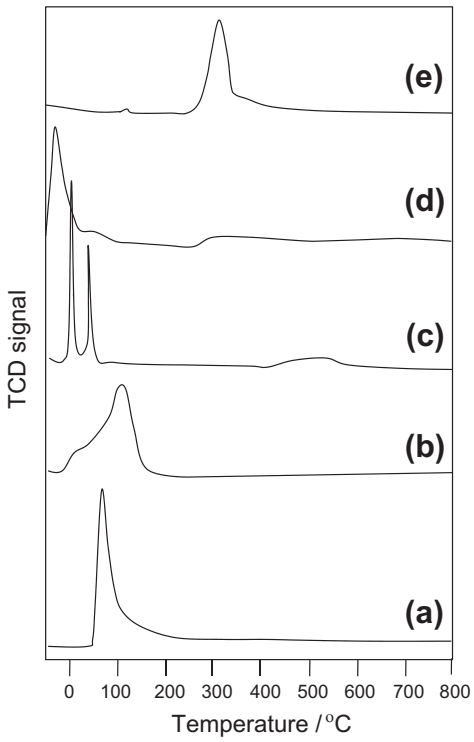

Fig. 4. Temperature-programmed reduction profiles for sequentially impregnated catalysts, (a) 4 wt%Pt–4 wt%Re/$CeZrO_4$, (b) 4 wt%Pt–4 wt%Re/Al_2O_3, (c) 4 wt%Pt–4 wt%Re/TiO_2, (d) 4 wt%Pt/TiO_2 and (e) 4 wt%Re/TiO_2.

3.4. Solvent effects

Fig. 5 shows the influence of solvent on the reaction time profile for the hydrogenation of *N*-methylpyrrolidin-2-one. There is a large solvent effect with the following rate order: hexane > tetrahydrofuran ~ diethyl ether > methanol > methyl *tert*-butyl ether. In all cases, the amine is the only product observed. There are a

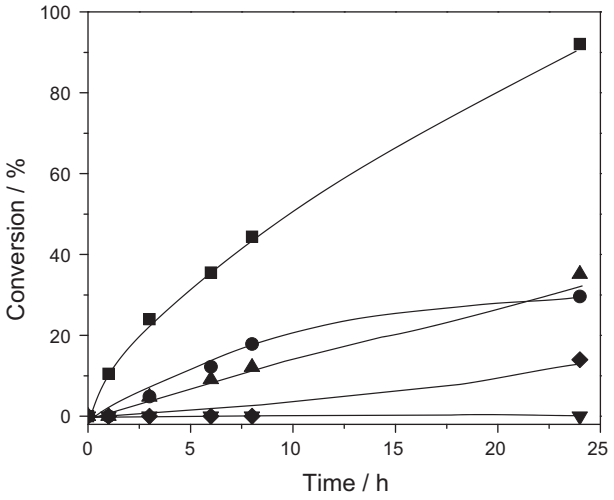

Fig. 5. Variation of amide conversion as a function of time for the hydrogenation of *N*-methylpyrrolidin-2-one at 120 °C, 20 bar H_2, stirred at 1500 rpm using 4 wt%Pt–4 wt%Re/TiO_2 in (■) hexane, (▲) tetrahydrofuran, (●) diethyl ether, (♦) methanol and (▼) methyl *tert*-butyl ether.

number of possible explanations for these solvent effects; for example the rate could be dependent on the concentration of hydrogen dissolved in each solvent or on the solubility of the amide in each solvent.

Table 2 shows the conversion after 24 h reaction time together with the hydrogen solubility [31] in each solvent and the E_T^N [32] solubility parameter, which provides a measure of the polarity of the solvent. From the values available, the rate of reaction is found to increase with the solubility of hydrogen in the solvent. Conversely, with the exception of the ether solvents, as the polarity of the solvent increases, the rate of reaction generally decreases. Although hydrogen solubility data are not available for the ether solvents, the Hildebrand solubility parameter, the square of which has been shown to correlate with the log of the hydrogen solubility, for diethyl ether is almost the same as hexane, 15.1 and 14.9, respectively [33], indicating that the change in rate is unlikely to be simply explained by either the hydrogen or amide solubility. However, it is interesting to note that the amide is less soluble in the non-polar hexane solvent and can adsorb strongly to the catalyst surface, whereas in polar solvents, partitioning between the surface and the solvent will mean that the concentration of the amide on the catalyst surface will be less resulting in a lower rate of reaction.

The strong adsorption of the amide on the surface in a non-polar solvent was demonstrated by contacting a pre-reduced catalyst with a hexane solution of amide in a nitrogen atmosphere for 3 h before reaction. Fig. S7 shows a decrease in the conversion from 92% after 24 h when H_2 was introduced at the start of the reaction to 30% when the catalyst was pre-treated with the substrate. This effect is attributed to the high surface coverage set up under the nitrogen atmosphere, thus inhibiting the access of the hydrogen to the surface. Conversely, when a similar experiment was carried out with the more polar THF, in which the amide is more soluble, only a small drop in conversion was observed, from 35% to 30%.

The formation of a mole of water for each mole of product formed could also contribute to the solvent effect observed, particularly in hydrophobic solvents such as hexane. Magnesium sulphate (58 mg) was, therefore, added to a reaction carried out in hexane using 4 wt%Pt–4 wt%Re catalysts supported on alumina, ceria-zirconia and titania, and small changes in the reaction rate were observed. In all cases, a slight increase in the reaction rate was found, albeit small; however, a detailed study needs to be undertaken to fully assess the effect of water on the rate. No change in the selectivity was observed following the addition of the drying agent.

3.5. Catalyst recycle

Although the reactions proceeded to completion under mild conditions over the fresh catalyst, with conversions of 92% being obtained in 24 h, the conversion decreased to 67% on the second run and to only 6% on the fifth run, when simply washed with solvent between each runs. Although drying and recalcination went someway to restore the initial activity with conversions increasing again to 53% and 30% after each treatment, respectively, the initial high activity was not completely regained. Any carbon present on the surface of the catalyst will have been removed by recalcination; therefore, the loss of activity may be attributed to decreased interaction between the platinum and rhenium.

Table 2
Comparison of the % conversion of *N*-methylpyrrolidin-2-one after 24 h using 4 wt%Pt–4 wt%Re/TiO_2 at 20 bar and 120 °C as a function of the solvent used and the hydrogen solubility and polarity parameter E_N^T for each solvent.

Solvent	%Conversion	$10^3 \times H_2$ at 20 bar and 25 °C [31]	Polarity parameter E_T^N [32]
Hexane	94	13.4	0.009
Tetrahydrofuran	35	5.4	0.207
Diethyl ether	30	–	0.117
Methanol	15	3.2	0.762
Methyl *tert*-butyl ether	0	–	0.124

3.6. Density Functional Theory (DFT) calculations

To obtain a general understanding of the trends of hydrogenation of *N*-methylpyrrolidin-2-one (MPDO), Scheme 1, DFT calculations were used to investigate the reaction mechanism on four transition metal surfaces (Re, Ru, Rh and Pt) with monatomic steps.

Amide hydrogenations can be initiated *via* one of three possible activation processes of the carbonyl bond, namely direct carbonyl bond cleavage, the cleavage with the assistance of the first hydrogenation of the carbonyl carbon or the first hydrogenation of the carbonyl oxygen. The subsequent step-wise hydrogenations of the intermediates after the carbonyl bond cleavage give rise to the two products, water and *N*-methylpyrrolidine (MPD). The free-energy profile for each metal under the reaction conditions (T = 120 °C, p_{H2} = 20 bar, $p_{MPDO} = 4.14 \times 10^{-3}$ bar being the vapour pressure of MPDO from an ideal solution) shows two striking features, as illustrated in Fig. 6. Firstly, the free-energy barrier of car-

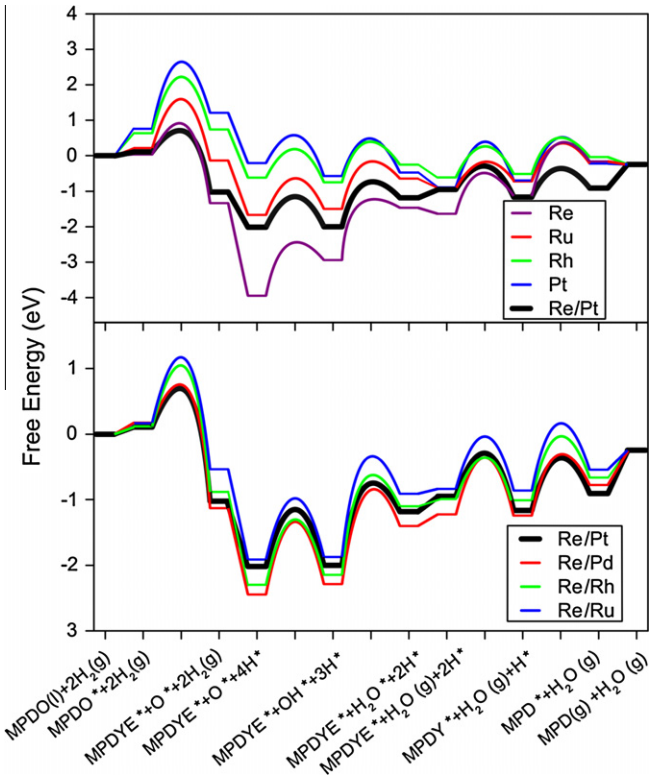

Fig. 6. Free-energy profiles of all intermediates and transition states in the hydrogenation of *N*-methylpyrrolidin-2-one (MPDO) to *N*-methylpyrrolidine (MPD) over different surfaces initiated by carbonyl dissocaition under realistic reaction conditions (T = 120 °C, p_{H2} = 20 bar, $p_{MPDO} = 4.14 \times 10^{-3}$ bar, 94% conversion). (a) Reaction over pure stepped Re, Ru, Rh and Pt sufaces, compared with a Re/Pt bimetallic system. (b) Reactions over bimetallic systems with an oxidised Re terrace on the substrate Pt, Pd, Rh and Ru. The preferential carbonyl activation mechanism on stepped Rh and Pt surfaces is via the first hydrogenation on carbonyl O, which is different from the others. However, as the difference in the C=O activation mechanism does not change the reactivity trend of the metal group, the data is plotted in terms of the C=O direct cleavage mechanism.

bonyl activation increases, whilst the overall barriers of the subsequent hydrogenations decrease in the order of the metal reactivities: Re, Ru, Rh and Pt. Secondly, the rate-determining step changes from carbonyl activation on Ru, Rh and Pt to the reduction of oxygen to water on Re. On the stepped Re surface, the overall activation barrier was found to be 2.74 eV, *i.e.* substantially higher than that found for the C=O bond breaking over the same surface (0.91 eV), implying that the hydrogenation of oxygen is the rate-determining step, Table S1. On all other metals examined, the activation of the C=O bond was found to be the most energy-demanding step. The free-energy barrier of direct C=O dissociation on Ru is 1.60 eV, which is sufficiently high to make activation under the reaction conditions very difficult, and this value was found to increase to 2.22 eV and 2.65 eV over the more inert Rh and Pt surfaces, respectively. It should be pointed out that the preferential carbonyl activation pathway on stepped Rh and Pt surfaces is via the first hydrogenation of the carbonyl oxygen followed by the C—OH cleavage instead of the direct C=O cleavage, which is preferred on stepped Re and Ru surfaces. This is in agreement with the DFT results from other groups and experimental studies, which show that on inert metal surfaces such as Pt and Pt-based bimetallic alloys, hydrogenation occurs readily to convert C=O to C—OH [34]. However, even with the assistance of hydrogen, the carbonyl activation barriers are still as high as 2.04 and 2.07 eV over stepped Rh and Pt surfaces, respectively, indicating that the rate-determining step on Rh and Pt is still the carbonyl activation.

To further understand the system, the energy barriers over a flat Re(0001) surface were compared with those over a stepped Re surface. Table S1 shows that on the flat Re(0001) surface, the C=O dissociation energy barrier is 2.11 eV, *i.e.* significantly higher than that on the step site. These results indicate that only low-coordination Re sites are capable of activating the C=O bond in MPDO. In addition, the overall barriers of subsequent hydrogenations on the flat Re surface were found to be as high as those on the stepped surface, implying that Re is a poor catalyst for the hydrogenation of the intermediates to products.

It is clear from these results why it is very difficult for pure metals to efficiently catalyse the hydrogenation of MPDO due to the balance between having sufficient oxophilicity to activate the C=O bond, whilst also enabling facile oxygen hydrogenation. In contrast, bimetallic catalysts can provide the necessary bifunctional sites to enable both the cleavage and the oxygen reduction, as shown for the Pt–Re catalytic system reported in this paper. This catalyst was modelled by a layer of Re with a size of (3×3) lying on a flat Pt(1 1 1) with p(5×3) unit cell as shown in Fig. 7, where Re was covered with 1 monolayer of oxygen, excluding the step edge sites at the Re/Pt interface. According to the calculated overall barrier (2.88 eV, see Table S1), the adsorbed oxygen is very difficult

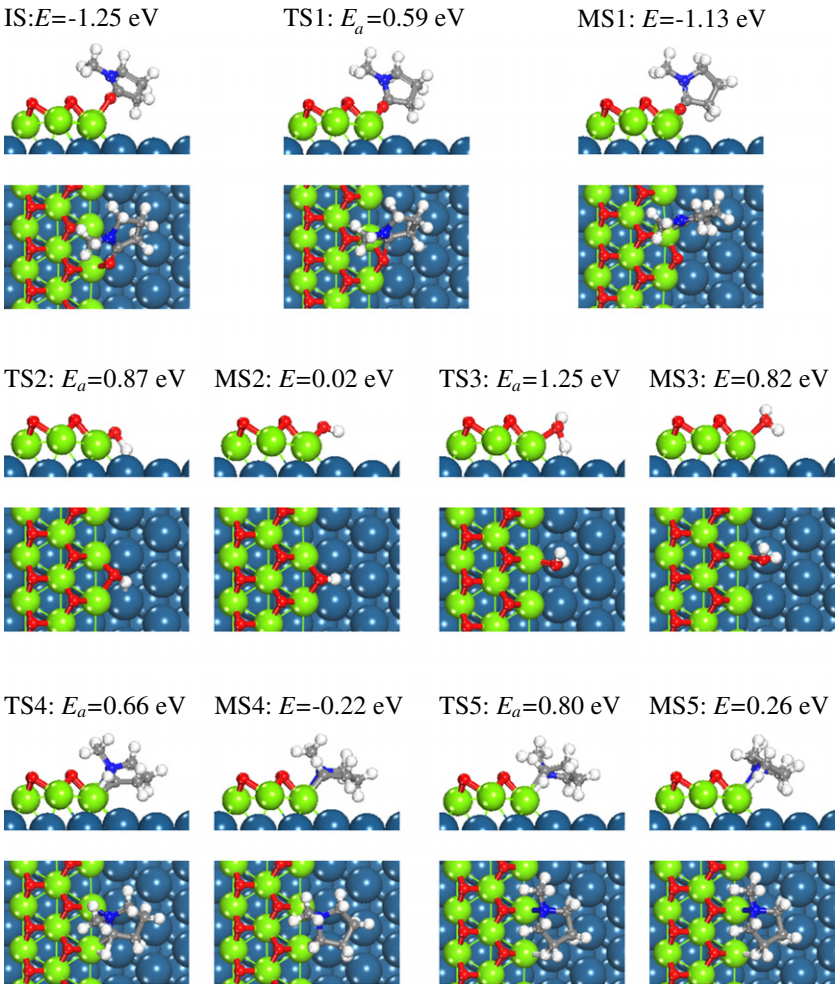

Fig. 7. Schematic representation of the side and top view of the initial states (IS), transition states (TS) and Intermediates (MS) in the hydrogenation of *N*-methylpyrrolidin-2-one (MPDO) on a Re/Pt surface and their corresponding energy barrier or reaction energy in each elementary step. The top, middle and bottom lines illustrate C=O activation, oxygen and *N*-methylpyrrolidin-2-ylidene (MPDYE) step-wise hydrogenation processes, respectively. The white, grey, blue and red balls and stick style indicate H, C, N and O atoms, respectively. The green and blue balls in CPK style are Re and Pt, respectively. (For interpretation of the references to colour in this figure legend, the reader is referred to the web version of this article.)

to hydrogenate to water on a flat Re surface under mild reaction conditions used here. In contrast, the adsorbed oxygen on Re step edge sites at the Re/Pt interface can be readily removed either via diffusion to the neighbouring terrace Re sites or by being hydrogenated to water. This is in agreement with the TPR results, which show a significant decrease in the temperature of ReO_x reduction in the presence of Pt, which is almost certainly due to strong electronic perturbation of the Re by the Pt. Similar effects have been reported previously and have recently been reviewed [35].

Fig. 7 shows that MPDO initially adsorbs atop on the step edge site of oxygen-covered Re with a binding energy of −1.25 eV (the corresponding free adsorption energy is 0.11 eV). The C═O bond was found to be easily split to yield adsorbed O and 1-methylpyrrolidin-2-ylidene (MPDYE) via TS1 with a low barrier of 0.59 eV (the corresponding free energy barrier of C═O activation with respect to liquid MPDO is 0.70 eV, Table S1), which is 0.21 eV lower than that on the Re stepped surface (0.91 eV on Re stepped surface).

The adsorbed hydrogen for subsequent hydrogenation steps was assumed to come mainly from the Pt lower terrace surface for the following reasons. Firstly, the C═O dissociation barrier on Re step edge sites on Re/Pt was found to be moderate, and the dissociation was strongly exothermic, leading to high coverage of oxygen and MPDYE, and very low coverage of adsorbed hydrogen. Secondly, MPDO does not adsorb onto a Pt terrace according to the calculated results on Pt(1 1 1), meaning that the Pt surface should be almost covered with adsorbed hydrogen for the subsequent hydrogenation steps. There are two possible pathways for the hydrogenation processes over the two-phase catalyst system:

(i) the hydrogen from Pt directly attacks the intermediates on the Re step edge sites via the Re–Pt interface; or
(ii) the adsorbed intermediates diffuse from the Re sites to Pt sites and are then reduced.

Mechanism (i) is favoured, as the overall barriers of hydrogenation of oxygen and MPDYE decrease to 1.27 and 0.66 eV, respectively, Table S1, compared with 2.74 eV and 2.00 eV, respectively, for pure Re step sites. Furthermore, higher hydrogenation coverages further promote the hydrogenation reaction rate. In mechanism (ii), the chemisorption energies of intermediates on the Pt terrace are much less favourable than the high chemisorption energies of intermediates on the step edge sites of Re on Re/Pt, Table S2. For the intermediates to migrate from Re to Pt, the diffusion barrier would have to be larger than the chemisorption energy difference between the two sites. As the diffusion barrier of the intermediates from Re to Pt (mechanism (ii)) is larger than the overall hydrogenation barrier in mechanism (i), mechanism (i) would be favoured in this system.

It is clear that the introduction of Pt as a second component forming a two-phase catalyst greatly decreases the hydrogenation barriers compared with those on pure Re surfaces. However, the C═O activation energy barrier is also slightly lowered on Re/Pt relative to that found on the Re stepped surface, further contributing to the ease with which this reaction can take place on this two-phase surface as compared with the pure metal catalysts. Similar analysis using Pd, Rh and Ru in combination with Re showed that the surfaces were less active than found with Pt. For example, although the combination of Re/Pd results in a C═O activation of free-energy barrier similar to that found for Re/Pt, Table S1, the overall barriers for the subsequent hydrogenation of oxygen and MPDYE were 0.33 and 0.26 eV higher than those found on Re/Pt. In the case of Re/Rh and Re/Ru, the free-energy barriers for C═O dissociation were found to be about 0.3–0.5 eV higher than those on Re/Pt and Re/Pd, whilst the overall barriers of subsequent hydrogenation reactions were close to those on Re/Pd. It can be concluded that the effectiveness of the second component metal is in the order Pt > Pd > Rh ∼ Ru. This is in good agreement with previously reported results on Ru/Re and Rh/Re bimetallic catalyst systems, which showed that, although the reduction of *N*-acetylpiperidine could be achieved, the reaction required 100 bar H_2 pressure and >150 °C [11].

4. Conclusions

Pt–Re bimetallic catalysts have been shown to be able to reduce *N*-methylpyrrolidin-2-one to *N*-methylpyrrolidine at low temperatures and moderate pressures (120 °C and 20 bar H_2 pressure) for the first time. The interaction between the Pt and Re was found to be critical in forming active amide hydrogenation catalysts. Although a range of supports was found to be effective for the hydrogenation, the use of titania was found to promote the activity of the bimetallic Pt/Re catalyst resulting in over 90% conversion and >99% selectivity to the corresponding amine after 24 h. Density functional theory calculations clearly demonstrated that the role of the Re was to activate the C═O bond, whereas the Pt aided the reduction of the Re—O and enabled the formation of water and the amine. Monometallic systems were shown not to provide the appropriate bifunctional capability.

Acknowledgments

The authors thank the EPSRC and Johnson Matthey plc for funding this work as part of the CARMAC (GR/S43702/01) and CASTech (EP/G012156/1) projects. LMcL acknowledges studentship funding from DELNI.

Appendix A. Supplementary material

Supplementary data associated with this article can be found, in the online version, at doi:10.1016/j.jcat.2011.07.007.

References

[1] G. Smith, F. Notheisz, Heterogeneous Catalysis in Organic Chemistry, first ed., Academic Press, 1999.
[2] J. March, Advanced Organic Chemistry, fourth ed., Wiley, New York, 1992. 1212.
[3]] H.C. Brown, S. Narasimhan, Y.O.N.G.M. Choi, Synthesis (1981) 441–442.
[4] H.C. Brown, P. Heim, J. Org. Chem. 38 (1973) 912–916.
[5] Z.B. Papanastassiou, J.B. Robert, J. Org. Chem. 29 (1964) 2870–2872.
[6] (a) B. Wojcik, H. Adkins, J. Am. Chem. Soc. 56 (1934) 247–248; (b) J.H. Paden, H. Adkins, J. Am. Chem. Soc. 58 (1926) 2487–2499; (c) J.C. Sauer, H. Adkins, J. Am. Chem. Soc. 60 (1938) 402–406.
[7] H.S. Broadbent, W.J. Bartley, J. Org. Chem. 28 (1963) 2345–2347.
[8] A. Guyer, A. Bieler, G. Gerliczy, Helv. Chim. Acta 38 (1955) 1649–1654.
[9] F. Galinovsky, E. Stern, Chem. Ber. 76 (1943) 1034–1038.
[10] I.D. Dobson, Eur. Patent, 286 280, 1988 (British Petroleum).
[11] C. Hirosawa, N. Wakasa, T. Fuchikami, Tetrahedron Lett. 37 (1996) 6749–6752.
[12] A.A. Smith, P. Dani, P.D. Higginson, A.J. Pettman, International patent WO2005/066112, 2005 (Avantium International).
[13] M.J. Nepras, R.J. Bernhardt, C.J. Sporer, United States Patent 5 840,985, 1998.
[14] (a) G. Beamson, A.J. Papworth, C. Philipps, A.M. Smith, R. Whyman, J. Catal. 269 (2010) 93–102; (b) G. Beamson, A.J. Papworth, C. Philipps, A.M. Smith, R. Whyman, J. Catal. 278 (2011) 228–238.
[15] E. Balaraman, B. Gnanaprakasam, L.J.W. Shimon, D. Milstein, J. Am. Chem. Soc. 132 (2010) 16756–16758.
[16] J.P. Perdew, K. Burke, M. Ernzerhof, Phys. Rev. Lett. 77 (1996) 3865–3868.
[17] G. Kresse, J. Hafner, Phys. Rev. B 49 (1994) 14251–14269.
[18] G. Kresse, J. Furthmüller, Comput. Mater. Sci. 6 (1996) 15–50.
[19] G. Kresse, D. Joubert, Phys. Rev. B 59 (1999) 1758–1775.
[20] A. Alavi, P. Hu, T. Deutsch, P.L. Silvestrelli, J. Hutter, Phys. Rev. Lett. 80 (1998) 3650–3653.
[21] A. Michaelides, P. Hu, J. Am. Chem. Soc. 123 (2001) 4235–4242.
[22] Z.-P. Liu, P. Hu, J. Am. Chem. Soc. 125 (2003) 1958–1967.
[23] P.W. Atkins, Physical Chemistry, Oxford University Press, Oxford, UK, 1998.
[24] M.J. Mendes, O.A.A. Santos, E. Jordão, A. Silva, Appl. Catal. A 217 (2001) 253–262.
[25] W. Rachmady, M.A. Vannice, J. Catal. 192 (2000) 322–334.
[26] T. Huizinga, J. Van Grondelle, R. Prins, Appl. Catal. 10 (1984) 199–213.
[27] K.G. Azzam, I.V. Babich, K. Seshan, L. Lefferts, J. Catal. 251 (2007) 163–171.
[28] J. Fan, X. Wu, R. Ran, D. Weng, Appl. Surf. Sci. 245 (2005) 162–171.

[29] S.M. Augustine, M.S. Nache, C.M. Tsang, J.B. Butt, W.M.H. Sachtler, in: M.J. Phillips, M. Ternan (Eds.), Proc. 9th Int. Congr. Catal., Chemical Institute of Canada, Calgary, 1988.
[30] J. Sá, C. Kartusch, M. Makosch, C. Paun, J.A. van Bokhoven, E. Kleymenov, J. Szlachetko, M. Nachtegaal, H. Manyar, C. Hardacre, Chem. Commun. 47 (2011) 6590–6592.
[31] (a) E. Brunner, J. Chem. Eng. Data 30 (1985) 269–273;
(b) T. Katayama, T. Nitta, J. Chem. Eng. Data 21 (1976) 194–196.
[32] C. Reichardt, Solvents and Solvent Effects in Organic Chemistry, third ed., Wiley-VCH, Weinheim, 2003. 472.
[33] A.F.M. Barton, Handbook of Solubility Parameters and Other Cohesion Parameters, second ed., CRC Press Inc., Florida, 1991. 250, 267.
[34] (a) D. Loffreda, F. Delbecq, F. Vigné, P. Sautet, J. Am. Chem. Soc 128 (2006) 1316–1323;
(b) L.E. Murillo, A.M. Goda, J.G. Chen, J. Am. Chem. Soc 129 (2007) 7101–7105.
[35] J.G. Chen, C.A. Menning, M.B. Zellner, Surf. Sci. Reports 63 (2008) 201–254.